Niu Zhou[1]
Chunmei Fan[1]
Song Liu[1]
Jianwei Zhou[1]
Yulan Jin[1]
Xiaojuan Zheng[1]
Qin Wang[4]
Jue Liu[5]
Hanchun Yang[6]
Jinyan Gu[1,2]*
Jiyong Zhou[1,3]

[1]Key Laboratory of Animal Virology of Ministry of Agriculture, College of Animal Sciences, Zhejiang University, Hangzhou, PR China
[2]Institute of Immunology and College of Veterinary Medicine, Nanjing Agricultural University, Nanjing, PR China
[3]State Key Laboratory and Collaborative Innovation Center for Diagnosis and Treatment of Infectious Diseases, First Affiliated Hospital, Zhejiang University, Hangzhou, PR China
[4]China Institute of Veterinary Drug and Control, Beijing, PR China
[5]Institute of Animal Husbandry and Veterinary Medicine, Beijing Academy of Agriculture and Forestry Sciences, Beijing, PR China
[6]College of Veterinary Medicine, China Agricultural University, Beijing, PR China

Received December 14, 2016
Revised February 21, 2017
Accepted February 21, 2017

Research Article

Cellular proteomic analysis of porcine circovirus type 2 and classical swine fever virus coinfection in porcine kidney-15 cells using isobaric tags for relative and absolute quantitation-coupled LC-MS/MS

Viral coinfection or superinfection in host has caused public health concern and huge economic losses of farming industry. The influence of viral coinfection on cellular protein abundance is essential for viral pathogenesis. Based on a coinfection model for porcine circovirus type 2 (PCV2) and classical swine fever virus (CSFV) developed previously by our laboratory, isobaric tags for relative and absolute quantitation (iTRAQ)-coupled LC-MS/MS proteomic profiling was performed to explore the host cell responses to PCV2-CSFV coinfection. Totally, 3932 proteins were identified in three independent mass spectrometry analyses. Compared with uninfected cells, 304 proteins increased (fold change >1.2) and 198 decreased (fold change <0.833) their abundance in PCV2-infected cells ($p < 0.05$), 60 and 61 were more and less abundant in CSFV-infected cells, and 196 and 158 were more and less abundant, respectively in cells coinfected with PCV2 and CSFV. Representative differentially abundant proteins were validated by quantitative real-time PCR, Western blotting and confocal laser scanning microscopy. Bioinformatic analyses confirmed the dominant role of PCV2, and indicated that mitochondrial dysfunction, nuclear factor erythroid 2-related factor 2 (Nrf2)-mediated oxidative stress response and apoptosis signaling pathways might be the specifical targets during PCV2-CSFV coinfection.

Keywords:
Classical swine fever virus / Coinfection / iTRAQ / Mitochondrial dysfunction / Porcine circovirus type 2
DOI 10.1002/elps.201600541

Additional supporting information may be found in the online version of this article at the publisher's web-site

1 Introduction

With the rapid advance in global communication and connectivity, viral coinfection or superinfection has become a worldwide threat. Coinfection involves the combination of more than one pathogen or strain, and can include infection with two or more viruses of the same type, by closely related types, or by completely different virus species or strains [1]. It is widely believed that coinfection of hepatitis B and C viruses (HBV and HCV, respectively) can have a synergistic effect in hepatocarcinogenesis by accelerating the development of hepatocellular carcinoma, one of the most common cancers in the world [2]. Similarly, coinfection of influenza A viruses in individuals and populations is considered the source of emerging novel assortment subtypes such as H7N9 [3], H10N8 [4], H17N10 [5], and H18N11 [6], which represent a potentially serious threat to public health and animal husbandry. In addition to influenza A viruses, numerous other viral pathogens are highly epidemic in swine herds, especially in developing countries, examples of which include porcine

Correspondence: Prof. Jiyong Zhou, Key Laboratory of Animal Virology of Ministry of Agriculture, College of Animal Sciences, Zhejiang University, Hangzhou 310058, PR China
E-mail: jyzhou@zju.edu.cn or jyzhou@njau.edu.cn

Abbreviations: CLSM, confocal laser scanning microscopy; **CSFV**, classical swine fever virus; **GO**, Gene Ontology; **HBV**, hepatitis B virus; **IFA**, indirect immunofluorescence assay; **IPA**, Ingenuity Pathways Analysis; **iTRAQ**, isobaric tags for relative and absolute quantitation; **KEGG**, Kyoto Encyclopedia of Genes and Genomes; **MOI**, multiplicities of infection; **PCV2**, porcine circovirus type 2

*Additional corresponding authors: Dr. Jinyan Gu
E-mails: gjy@njau.edu.cn

Colour Online: See the article online to view Figs. 1–8 in colour.

reproductive and respiratory syndrome virus (PRRSV), porcine parvovirus (PPV), classical swine fever virus (CSFV) and porcine circovirus type 2 (PCV2). Coinfection of two or even more viruses in swine individuals is common and results in huge economic losses to the swine production industry.

The immunosuppressive virus PCV2 is a member of the genus *Circovirus* of the family *Circoviridae*, and this non-enveloped virus contains an ambisense, single-stranded, closed-circular genome ranging from 1766 to 1768 nucleotides [7, 8]. PCV2 is the main agent of porcine circovirus diseases (PCVD) or PCV2-associated diseases (PCVAD) [9].

CSFV is a member of the genus *Pestivirus* in the family *Flaviviridae*, and this small, enveloped virus is non-segmented and has a single-stranded positive RNA genome [10]. CSFV is the causative agent of classical swine fever, also known as hog cholera, which is notifiable to the World Organization for Animal Health (OIE). Multiple clinical cases of PCV2 and CSFV coinfection have been reported, and PCV2 infection was found to interfere with the protective efficacy of an attenuated CSFV vaccine in field experiments [11]. Our recent study also revealed that PCV2 and CSFV coinfection occurred within the single cell in vitro, and PCV2 interfered CSFV replication [12]. However, the potential molecular mechanism involved in the coinfection of these two viruses remains unknown.

As efficient methods for large-scale screening, quantitative proteomic approaches are widely used to explore changes in host proteins in response to viral infection [13]. Methods include 2DE [14], 2D-DIGE [15], stable isotope labeling with amino acids in cell culture (SILAC) [16], iTRAQ [17] and label-free proteomic techniques [18]. These techniques have inherent advantages and limitations, and are therefore complementary [19]. For example, iTRAQcan be combined with LC-MS/MS to allow four or more samples to be analyzed simultaneously, which improves peptide identification coverage and accuracy [20] and significantly reduces the time required for MS analysis, in addition to lowering chemical noise and variation between individual experiments [21].

To follow on from our recent study, in the present work we investigated the cellular responses to PCV2 and CSFV coinfection. Based on our previous coinfection model of PCV2 and CSFV, three independent comparative proteomic experiments were performed using 4-plex iTRAQ reagents, which identified 3932 proteins in porcine kidney-15 (PK15)-infected cells. Differentially abundant proteins were determined, and hierarchical cluster and bioinformatic analyses demonstrated a dominant role for PCV2 in PCV2-CSFV coinfection. To illuminate the impact of PCV2 on CSFV during coinfection, KEGG and IPA analysis of differentially abundant proteins revealed potentially important roles for host proteins 14-3-3 ζ, cullin 3, ERK1/2, caspase and NFκB in mediating the effect of PCV2 on the life cycle of CSFV in vitro. Furthermore, bioinformatic analysis of specific differentially abundant proteins suggested that mitochondrial dysfunction and the oxidative stress response mediated by nuclear factor erythroid 2-related factor 2 (Nrf2, also NFE2L2) might be the specifical targets of PCV2-CSFV coinfection.

2 Materials and methods

2.1 Cells, viruses, and antibodies

The PCV-free porcine kidney epithelial cell line (PK15) [22] and PK15 cells harboring the replicating CSFV HCLV-strain (PK15-CSFV) [12] were kept in our laboratory and maintained in minimal essential medium (MEM; Gibco, Carlsbad, CA) containing 10% gamma-irradiated fetal bovine serum (FBS; Gibco). PCV2 strain HZ0201 (AY188355; $10^{6.4}$ $TCID_{50}$ / 0.1 mL) isolated from a pig with naturally occurring PMWS was propagated in PK15 cells [8]. A polyclonal antibody (pAb) and monoclonal antibody (mAb) against the PCV2 Cap protein [23], and a pAb against the CSFV N^{pro} protein were obtained as previously described, and mAb WH303 raised against CSFV E2 protein [24] was kindly gifted by Prof. Trevor Drew of Animal and Plant Health Agency (former Veterinary Laboratories Agency, Weybridge, UK).Primary antibodies against macrophage migration inhibitory factor (MIF; ab175189, rabbit mAb; Abcam, Cambridge, MA), heterogeneous nuclear ribonucleoprotein A2/B1 (hnRNPA2B1; ab6102, mouse mAb; Abcam), ferritin heavy chain (FTH1, ab65080, rabbit pAb; Abcam), CCAAT / enhancer binding protein delta (CEBPD; ab65081, rabbit pAb; Abcam) or histone H3 (R1105-1, rabbit pAb; Huabio, Hangzhou, China), and secondary antibodies conjugated with Alexa Fluor 546, Alexa Fluor 647 (Life Technologies, Gaithersburg, MD), FITC, or HRP (KPL, Gaithersburg, MD) were obtained from commercial suppliers.

2.2 Virus inoculation

Cells (>90% confluent) were subcultured, inoculated directly with PCV2 at the indicated multiplicities of infection (MOI), and maintained at 37°C with 5% CO_2. After culturing for the specified time period, cells were fixed for examination of viral infection by indirect immunofluorescence assay (IFA), collected for total RNA extraction to determine the mRNA levels of genes by absolute quantitative real-time PCR, or lysed to determine protein abundance profiles by iTRAQ and immunoblotting.

2.3 IFA and confocal laser scanning microscopy (CLSM)

IFA and CLSM were performed as previously described [12]. Briefly, cells were inoculated with virus for indicated times, washed twice with PBS, fixed with a methanol-acetone mixture (1:1, v/v) at -20°C for 20 min, blocked with 5% skimmed milk in PBS at 37°C for 1 h, and incubated with antibodies at 4°C overnight or at room temperature (RT) for 1 h. Cellular nuclear DNA were stained with 4′-6-diamidino-2-phenylindole (DAPI) (Roche, Mannheim, Germany) at RT for 5 min. For IFA, mouse mAbs against PCV2 Cap or CSFV E2 were used as primary antibodies, followed by incubation with FITC-conjugated secondary antibodies. Images of

stained cells were observed and captured using an IX71 inverted fluorescence microscope and related software (Olympus, Tokyo, Japan). Viral infection rates in cell lines were analyzed using ImageJ software. For CLSM, primary antibodies included swine pAb anti-PCV2 Cap, mouse mAb anti-CSFV E2 and rabbit pAbs anti-FTH1 or anti-CEBPD. After gentle washing, cells were incubated with FITC-conjugated goat anti-swine IgG (KPL), Alexa Fluor 647-conjugated donkey anti-mouse IgG (Life Technologies) and Alexa Fluor 546-conjugated donkey anti-rabbit IgG (Life Technologies) as secondary antibodies. Cells were visualized with a Zeiss LSM780 confocal laser scanning microscope and ZEN 2012 software (Zeiss, Oberkochen, Germany).

2.4 Protein preparation and digestion

PK15 and PK15-CSFV infected with or without PCV2 were collected, lysed with SDT buffer (4% SDS w/v, 0.1 M DTT, 0.15 M Tris-HCl, pH 8.0) and ultrasonicated at 100 W for 10 min in pulses of 10 s with 15 s pauses. Samples were centrifuged at 12 000 × *g* for 10 min at 4°C, and supernatants were collected and stored at -80°C until needed. Protein digestion was performed according to the filter-aided sample preparation (FASP) procedure as described previously [25], and the resultant peptide mixture were analyzed as described below.

2.5 Electrospray ionization mass spectrometry (ESI MS)

Peptide mixtures for digestion were prepared as described above and loaded on a Zorbax 300SB-C18 peptide trap (Agilent Technologies, Wilmington, DE) and separated on an EASY column (ProxeonBiosystems). MS analysis was performed on an LTQ Velos mass spectrometer (Thermo Fisher Scientific, San Jose, CA) with a m/z range from 300 to 1800, and full-scan MS base peak chromatograms were recorded for all peptides.

2.6 iTRAQ labeling, fractionation, and liquid chromatography-tandem MS (LC-MS/MS) analysis

Using the 4-plex iTRAQ reagents according to the manufacturer's instructions (Applied Biosystems, Foster city, CA), peptide mixtures were respectively labeled as mock-infected (NE)-114/117/116, PCV2-infected (SP)-115/116/117, CSFV-infected (SC)-116/115/114 and PCV2-CSFV coinfection (PC)-117/114/115. Protein samples from independent experiments were mixed, vacuum dried and fractionated by strong cation exchange chromatography using an AKTA Purifier 100 system (GE Healthcare) and analyzed on a Q Exactive mass spectrometer coupled with an EASY nLC system (ProxeonBiosystems, now Thermo Fisher Scientific) as described previously [26].

2.7 Sequence database searching and data analysis

MS/MS spectra were searched using the MASCOT engine (version 2.2; Matrix Science, London, UK) embedded within Proteome Discoverer 1.3 (Thermo Electron, San Jose, CA) against the UniProt*Susscrofa* database (55 598 sequences, downloaded on February 20, 2014), the UniProt CSFV database (1356 sequences, downloaded on December 31, 2013) and the UniProt PCV2 database (2234 sequences, downloaded on December 31, 2013). For protein identification, the following options were used: Peptide mass tolerance = 20 ppm, MS/MS tolerance = 0.1 Da, enzyme = trypsin, missed cleavage = 2, fixed modification: carbamidomethyl (C), iTRAQ 4-plex (K), iTRAQ 4-plex (N-term), variable modification: oxidation (M), false discovery rate ≤0.01. Data were deposited at ProteomeXchange [27] via the PRIDE database [28] using submission tool version 2.3.2. Fold changes and *p* values were analyzed using Microsoft Excel 2013. Proteins with a fold change ≥1.200 or ≤0.833 and a *p* value <0.05 were defined as differentially abundant.

2.8 Hierarchical cluster analysis

To evaluate the capability of identified proteins in differentiating samples, proteins with selective feature were determined using information gain attribute evaluation and correlation-based feature selection in WEKA data mining software [29], and analyzed by hierarchical cluster as previously described [30].

2.9 Bioinformatic analyses of Gene Ontology (GO) and Kyoto Encyclopedia of Genes and Genomes (KEGG)

Sequence data from selected differentially abundant proteins were retrieved in batches from the UniProtKB database (Release 2014_04) in FASTA format. The retrieved sequences were locally searched against the SwissProt database (Mammal) using the NCBI BLAST 2.2.28 software to obtain sequences of homologs from which the functional annotation data could be extracted, and the identified sequences were then functionally annotated. In this study, the top 10 BLAST hits with an E-value less than 1E-3 for each query sequence were retrieved and loaded into Blast2GO (Version 2.7.1) for GO mapping and annotation. Following annotation and annotation augmentation, proteins were BLAST searched against the KEGG GENES database to retrieve KEGG Orthology identification (KO) entries and subsequently mapped to pathways in KEGG.

2.10 Ingenuity pathways analysis (IPA)

To obtain further insight into the functions of the identified differentially abundant proteins, pathways and molecular networks between groups were analyzed using IPA

(Ingenuity Systems, Redwood City, CA). Briefly, identified proteins were uploaded to the IPA software and mapped to their corresponding gene objects, and biological functions, canonical pathways and molecular networks of gene objects were subsequently evaluated and constructed based on information in the IPA database. Statistics for the functional analysis were calculated automatically by the software using the right-tailed Fisher's exact test. Molecular networks generated based on ranking scores were optimized to include as many proteins from input abundance profiles as possible, and to maximize network connections. Nodes in networks were coloured, and different shapes were used to represent fold changes and functional classes of genes and gene products. Interactions between nodes were connected only when supported by at least one or more references.

2.11 Relative quantitative PCR (qPCR)

To validate the changes in abundance of the proteins identified by iTRAQ, total mRNA was extracted from cells infected with one or both viruses using TRIzol reagent (Invitrogen, Carlsbad, CA) and reverse-transcribed using the SuperScript First-Strand Synthesis System (Fermentas, Pittsburgh, PA) according to manufacturer's instructions. The β-actin gene was used as an internal standard, and the relative quantitative abundance of selected genes was assayed by real-time PCR using the SYBR Premix Ex Taq (TaKaRa, Dalian, China) with an ABI 7500 sequence detection system (Applied Biosystems). The results were calculated as the mean value of triplicate reactions. Primers used for amplification of the selected genes are shown in Supporting Information Table S1.

2.12 Western blotting

To further verifythe changes in abundance of the proteins identified by iTRAQ, cells infected with viruses were collected, lysed in SDT buffer, and analyzed by Western blotting as previously described [31]. Briefly, protein samples were separated on 12% SDS-PAGE gels and transferred onto 0.22 μm nitrocellulose membranes (Amersham Biosciences, Berks, UK) using a semidry electrophoretic transfer cell (Bio-Rad Laboratories, Hercules, CA). Membranes were subsequently blocked in 5% (w/v) skimmed milk in PBS containing 0.05% Tween-20 for 1 h, and incubated with the indicated primary antibodies at 4°C overnight, followed by the corresponding HRP-conjugated antibodies for 1 h at RT. Bands on the membrane were visualized using the SuperSignal West Pico Trial Kit (Pierce, Rockford, IL) under a FluorChem M detection system (Cell Biosciences, Santa Clara, CA).

2.13 Venn diagram

Venn diagrams were constructed online (http://bioinfogp.cnb.csic.es/tools/venny/index.htmL) according to the introduction on the website.

2.14 Statistical method

Data are presented as mean ± SD of at least three individual experiments. Statistical differences between groups were analyzed by the unpaired *t*-test using Microsoft Excel 2013. A value of $p < 0.05$ was considered as statistically significant.

2.15 Ethics statement

The procedures used for the preparation of pAb and mAb in experimental animals were approved by the Institutional Animal Care and Use Committee (IACUC) of Zhejiang University (Permit No. SYXK 2012-0178), in accordance with the Regulations for the Administration of Affairs Concerning Experimental Animals approved by the State Council of PR China.

3 Results

3.1 Preparation of PCV2-CSFV coinfection samples for proteome analysis

To explore global proteomic changes following PCV2-CSFV coinfection and the mechanisms involved, PCV2 infection experiments were performed. Our recent study showed that there are no differences in the phenotype PK15 cells infected with PCV2 or coinfected with PK15-CSFV [12], therefore PK15 cells were inoculated with PCV2 at various MOI values and subjected to IFA analysis to determine the infection rate. As shown in Fig. 1A, the percentage of PCV2-positive cells reached a peak at 64 h post-inoculation (hpi), then decreased gradually. A higher PCV2 infection rate (>30%) at an MOI of 10 at 64 hpi was considered suitable and used for subsequent iTRAQ-based proteome analysis. IFA (Fig. 1B) and Western blotting (Fig. 1C) confirmed that samples were infected with a high titre of virus, and ESI MS (Fig. 1D) confirmed that parallel samples were consistent.

3.2 Identification and quantification of differentially abundant proteins by using iTRAQ-based LC-MS/MS

In total, 42664 unique peptides with false discovery rate <0.01 were identified from three biological replicate samples using LC-MS/MS analysis, which mapped to 5890 protein groups/proteins in the UniProt database (Supporting Information Tables S2 and S3, respectively). Representative MS/MS spectra of peptides from the identified putative differentially abundant proteins CEBPD and FTH1 from all 12 channels are shown in Supporting Information Fig. S1. Of the 5890 identified proteins, 12 were from the UniProt PCV2 database, one was from the UniProt CSFV database, and the rest were from the UniProt*Susscrofa* database. In every pair of replicates, more than 85% of the identified proteins

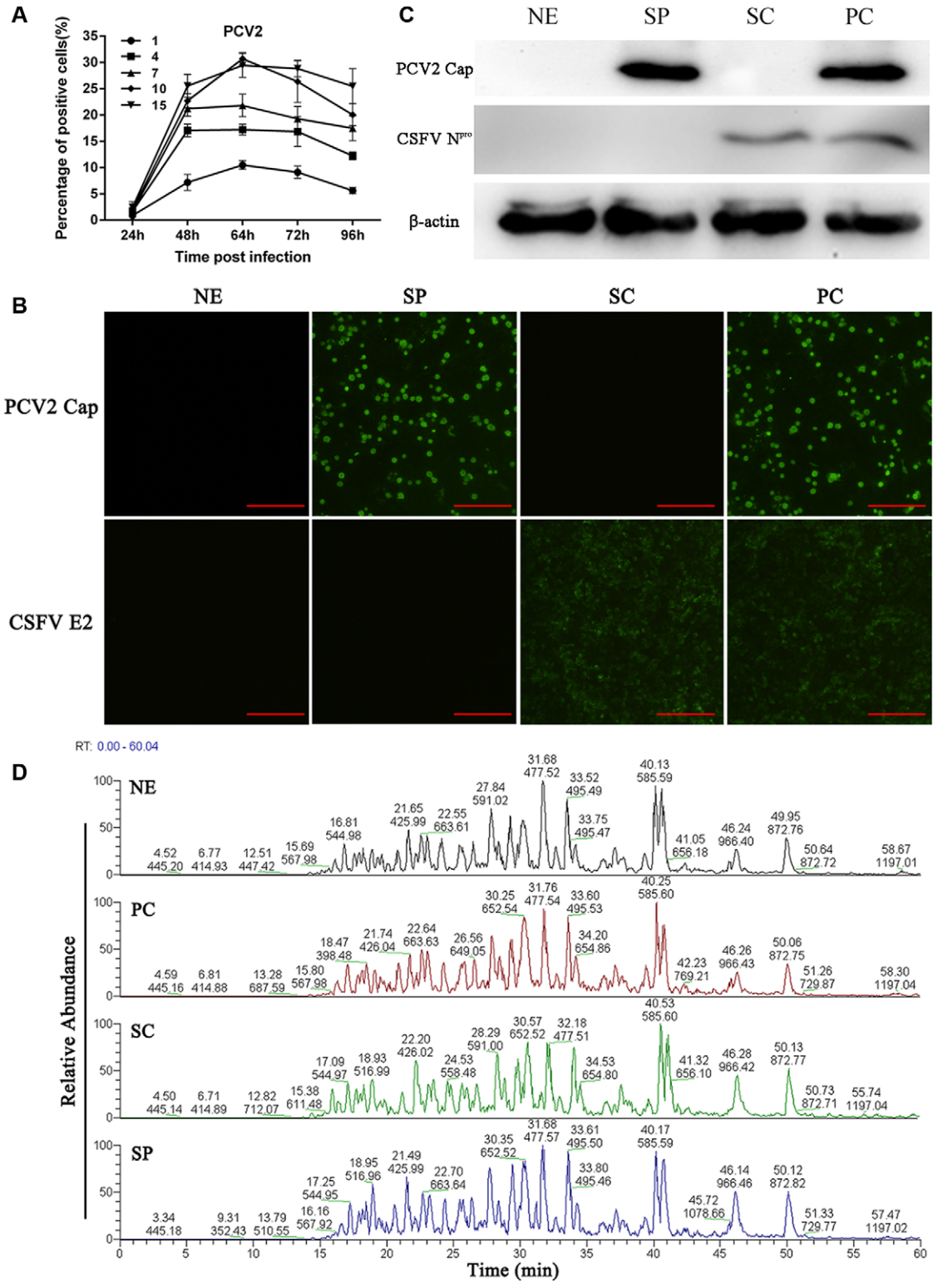

Figure 1. Viral infection and protein abundance profiles in cells. PK15 cells infected with PCV2 at the indicated MOIs were prepared for IFA and infection rates of PCV2 were calculated (A). PK15 and PK15-CSFV cells were infected with PCV2 at an MOI of 10 and cells were collected at 64 hpi and analyzed using IFA (B), Western blotting (C) and ESI mass spectrometry (D). Bar = 200 μm. NE, negative PK15. SP, PK15 infected with PCV2. SC, PK15-CSFV. PC, PK15-CSFV infected with PCV2. These experimental group names were used in all subsequent analyses.

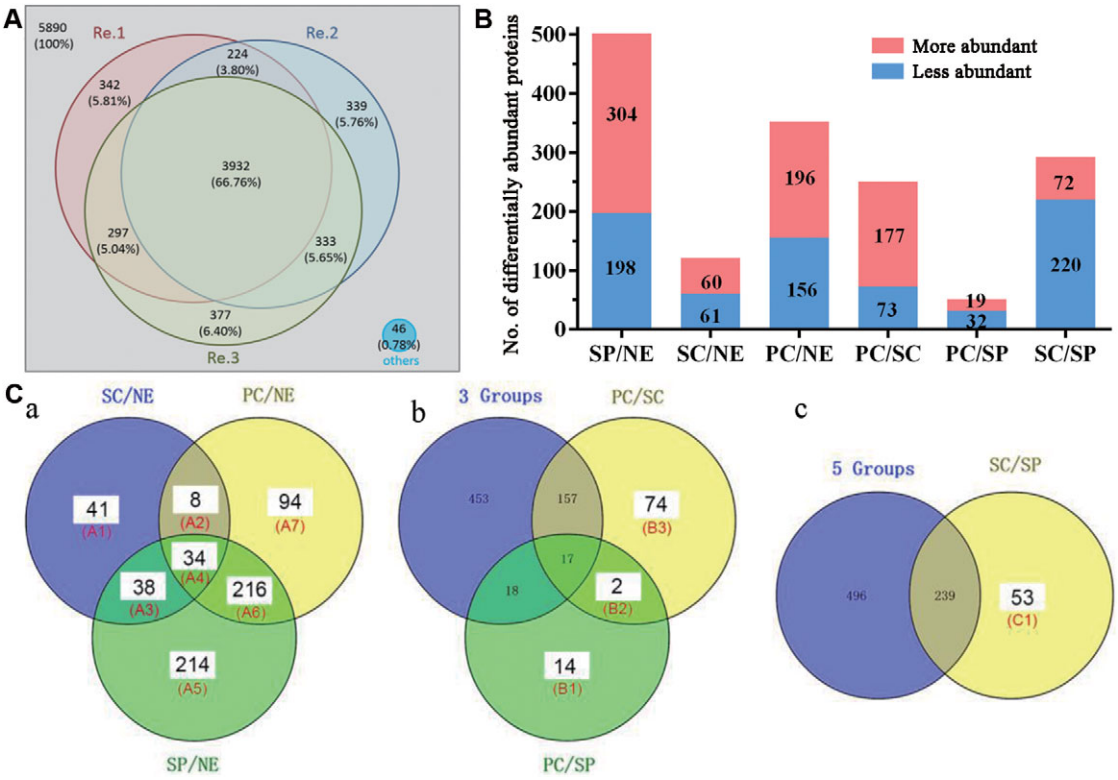

Figure 2. Analysis and clusters based on identified proteins with altered abundance. (A) Venn diagram proteins of identified in three independent experiments. Re.1, Re.2, and Re.3 represent each replicate. The number of proteins shown in each area and the percentage below indicate the number and the percentage of the total number (5890). (B) Number of proteins with altered abundance between groups. A total of 3932 proteins across three replicates were analyzed using a cutoff of ratio ≥1.200 or ≤0.833 (p<0.05). (C) Serial Venn diagram analyses of differentially abundant proteins between groups. (A) Venn diagram of SC/NE, PC/NE, and SP/NE. (B) Venn diagram of elements in a, PC/SC and PC/SP. (C) Venn diagram of elements in b and SC/SP. The number of differentially abundant proteins is shown under the respective cluster name.

overlapped (Supporting Information Table S4), confirming the results were of a high quality. In total, 3932 proteins were identified in all three biological replicates from the iTRAQ-based analysis (Fig. 2A). MS-derived data have been deposited in the ProteomeXchange Consortium [27] via the PRIDE partner repository [28] under the dataset identifier PXD005125.

The numbers of proteins that increased and decreased their abundance using a cutoff ratio of ≥1.200 or ≤0.833 (p<0.05) were summarized in Fig. 2B. Compared with mock-infected cells (NE), the number of proteins that differentially increased and decreased their abundance was 304 and 198 in PCV2-infected cells (SP), 60 and 61 in CSFV-infected cells (SC), and 196 and 156 in cells coinfected with PCV2 and CSFV (PC). In addition, 177 and 73 proteins were differentially more and less abundant in PC/SC, 19 and 32 in PC/SP, and 72 and 220 in SC/SP, respectively. Following serial Venn diagram analyses (Fig. 2C), 788 differentially abundant proteins were obtained across all groups and divided into 11 clusters (shown in the white box). Proteins uncharacterized in the UniProt database were mapped to the GO database to derive additional functional information (Supporting Information Table S5). Identification of a smaller number of differentially abundant proteins in SC/NE and PC/SP than in SP/NE and PC/SC (Fig. 2C and Supporting Information Table S5) suggested that infection with CSFV resulted in fewer changes in the global proteome of PK15 than did infection with PCV2.

3.3 Validation of iTRAQ-identified differentially abundant proteins

To validate the changes in abundance of the proteins detected byiTRAQ, cells infected with one or both viruses were subjected to qPCR, immunoblotting and CLSM analyses at 64 hpi. Of the 30 differentially abundant protein-encoding genes identified by qPCR, the abundance patterns of most (67.78%) were in accordance with the protein levels determined by iTRAQ (Fig. 3A). Immunoblotting analysis of five selected putative differentially abundant proteins (Fig. 3B) revealed that, compared with mock-infected PK15, FTH1 and monomer MIF (12 kDa) were more abundant in virus-infected cells, especially in PCV2-infected cells. However, there was no obvious alteration in trimeric MIF (37 kDa), and abundance of CEBPD, histone H3 and hnRNPA2B1

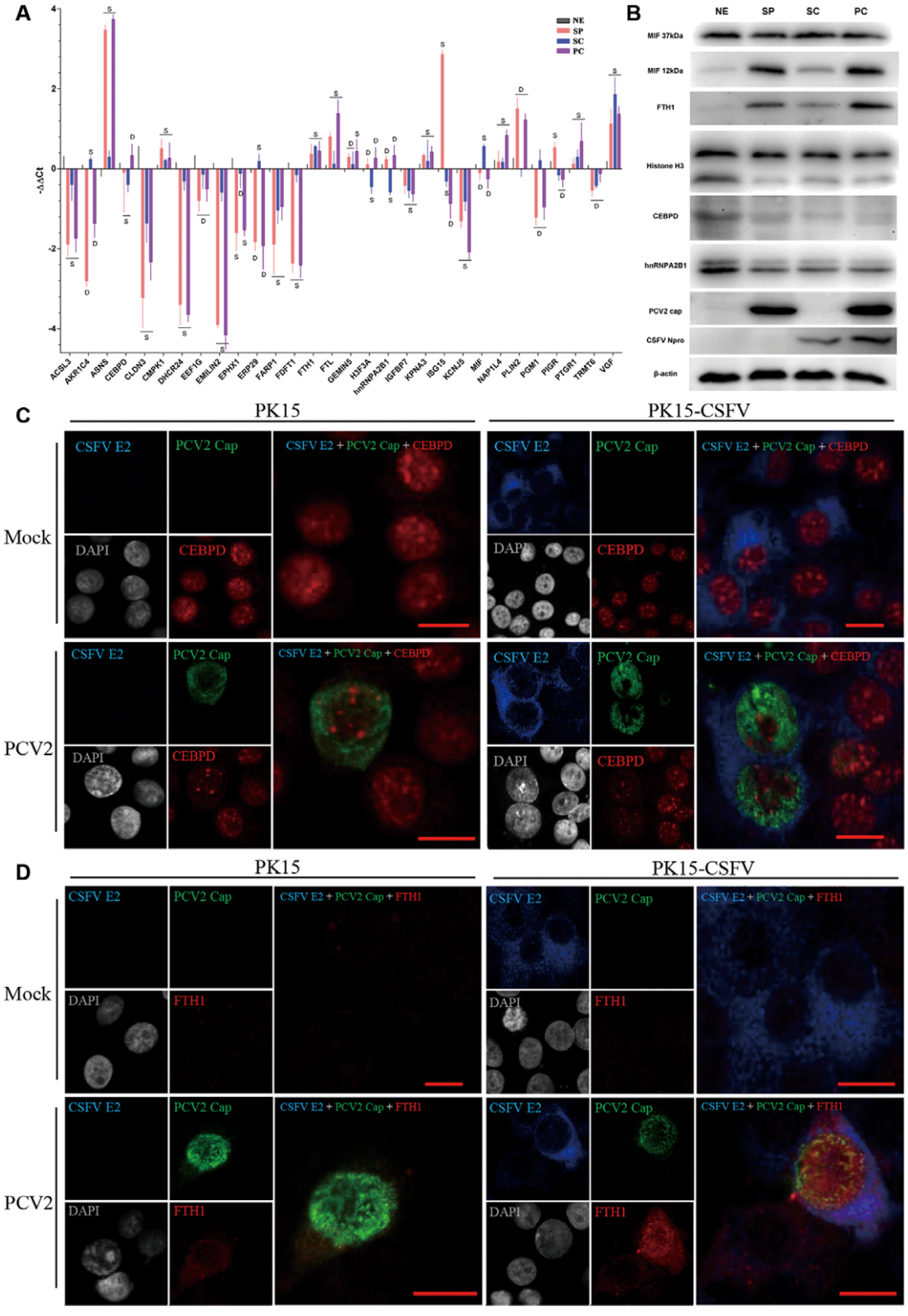

Figure 3. Validation of iTRAQ-identified differentially abundant proteins. Cells were infected with PCV2 (MOI = 1) and collected for validation after 64 h. (A) Transcriptional analysis of differentially abundant proteins following extraction and reverse-transcription of total cellular RNA. The β-actin gene was used as an internal standard. S and D above the pillars indicate the same and different abundance patterns compared with iTRAQ-based proteomic results, respectively. (B) Immunoblotting analysis of differentially abundant proteins. Cell samples were hybridized against MIF, FTH1, histone H3, CEBPD, hnRNPA2B1, β-actin, the Cap PCV2 protein and N^{pro} of CSFV, respectively. (C, D) CLSM analysis of CEBPD and FTH1. CSFV E2 (blue), PCV2 Cap (green), nucleus (grey) and CEBPD (C, red) or FTH1 (D, red) were localized. Bar = 10 μm.

decreased in virus-infected cells. Furthermore, CLSM visualization of the intracellular distribution of CEBPD and FTH1 proteins revealed that CEBPD was mainly located within the nuclei of PK15 and PK15-CSFV-infected (Fig. 3C), but was dispersed in cells infected with PCV2 (Fig. 3C). Meanwhile, FTH1 was present at basal levels in PK15 and PK15-CSFV-infected cells, but its abundance greatly increased within both the cytoplasm and nuclei of PCV2-infected cells (Fig. 3D). Taken together, these results confirmed the reliability of the iTRAQ-based proteome analysis.

3.4 Hierarchical cluster analysis of the identified proteins

To explore the abundance profiles and relationships between proteins across all 12 samples, hierarchical cluster analysis was carried out. Based on the proteome profiles, NE, SP, SC, and PC formed four minor clusters and two major clusters (Fig. 4), which indicated that NE was more closely related to SC, and PC was more closely related to SP. Furthermore, 56 proteins were categorized (Supporting Information Table S6), of which 39 were differentially abundant (Fig. 4, Ac. No. in red). Proteins in the same cluster were found to display similar abundance patterns, share similar characters, or take part in the same cellular processes. For instance, TUBA4A, TUBB3 and TUBB6 are all subunits of tubulin, and HSP90B1, CCT7, CCT8, and CCT6A work together during protein folding.

3.5 GO analysis of the differentially abundant proteins

Using the Blast2GO tool (version 2.7.1) and the GO Consortium website, GO annotation of cellular components was performed to derive molecular function and biological process information for differentially abundantproteins. In general, protein abundance profiles were similar for all identified proteins in terms of cellular components (Fig. 5A), molecular functions (Fig. 5B) and biological processes (Fig. 5C). Compared with cellular components of all identified proteins, the others varied from 4.30 to 7.87% as the result of viral infection. Regarding molecular functions, catalytic activity was present at 19.05% in SC/NE, 31.62% in SC/SP, and 24.68−29.0% in the others, and this variation indicated that CSFV was less dependent on host cellular enzymes for replication than was PCV2. However, compared with the others (2.15−4.34%), the percentage of proteins with transporter activity increased in SC/NE (10.58%) and PC/SP (6.49%), suggesting infection with CSFV alone or in combination with PCV2 significantly altered the abundance of proteins with transporter activity. Additionally, the differentially abundant proteins identified in SP/NEwere generally related to rhythmic processes, which might explain the observation of congenital tremors in piglets infected with PCVAD [32].

3.6 KEGG pathway analysis of the differentially abundant proteins

KEGG analysis was performed to obtain information on the biological pathways in which the differentially abundant proteins may be involved. The results showed that the number of related KEGG pathways (Fig. 6A) was in accordance with the number of differentially abundant proteins (Fig. 2B). Specifically, a greater number of pathways were associated with cells infected with PCV2 than with CSFV. Pathways with significant differences ($P<0.05$) in PC/NE, SC/NE, and SP/NE were analyzed using a Venn diagram (Fig. 6B), and a total of 76 pathways were categorized (Supporting Information Table S7), two of which were involved in all three groups. A total of 32 pathways were identified in both SP/NE and PC/NE, suggesting PCV2-CSFV coinfection affected the abundance of proteins in a greater number of pathways than did infection with PCV2 alone, and PCV2 appeared to play the dominant role during PCV2-CSFV coinfection.

3.7 IPA analysis of the differentially abundant proteins confirmed the dominant role of PCV2 in PCV2-CSFV coinfection

To investigate the impact of PCV2 on CSFV during coinfection, 250 differentially abundant proteins in PC/SC (Fig. 2B) were imported into the IPA software. Following exclusion of viral proteins, repeated proteins and uncharacterized proteins, 232 proteins were mapped and analyzed, and 73 biological functions and 65 canonical pathways were identified ($p<0.05$). The predominant biological functions involved in PC/SC were cellular growth and proliferation, cell death and survival, and neurological disease (Fig. 7A), and the major canonical pathways influenced by PCV2 infection were glycolysis I, gluconeogenesis I and ethanol degradation II (Fig. 7B). Among the canonical pathways, Nrf2-mediated oxidative stress response (Z-score = 1.633, ratio = 0.044) and PI3K/AKT signaling (Z-score = 1.000, ratio = 0.033) were predicted to be activated (data not shown).

To investigate the interactions among differentially abundant proteins, 14 molecular networks were constructed by IPA (Supporting Information Table S8) and neurological disease, psychological disorders, cancer (Fig. 7C), cellular movement, haematological disease, immunological disease (Fig. 7D) and cell morphology, cellular assembly and organization, and cellular compromise (Fig. 7E) were the dominant categories. Two of the differentially abundant proteins (14-3-3 ζ, encoded by *YWHAZ* and cullin, encoded by *CUL3*) were central nodes in the resulting molecular networks, and are known to play important roles in mediating signal transduction and degrading specific protein substrates by polyubiquitination, respectively. Additionally, although the abundance of some central node proteins like ERK1/2, caspase or NFκB (complex) didn't alter significantly, most of their immediate neighbors in the networks were differentially abundant, which might induce post-translation modification or changes

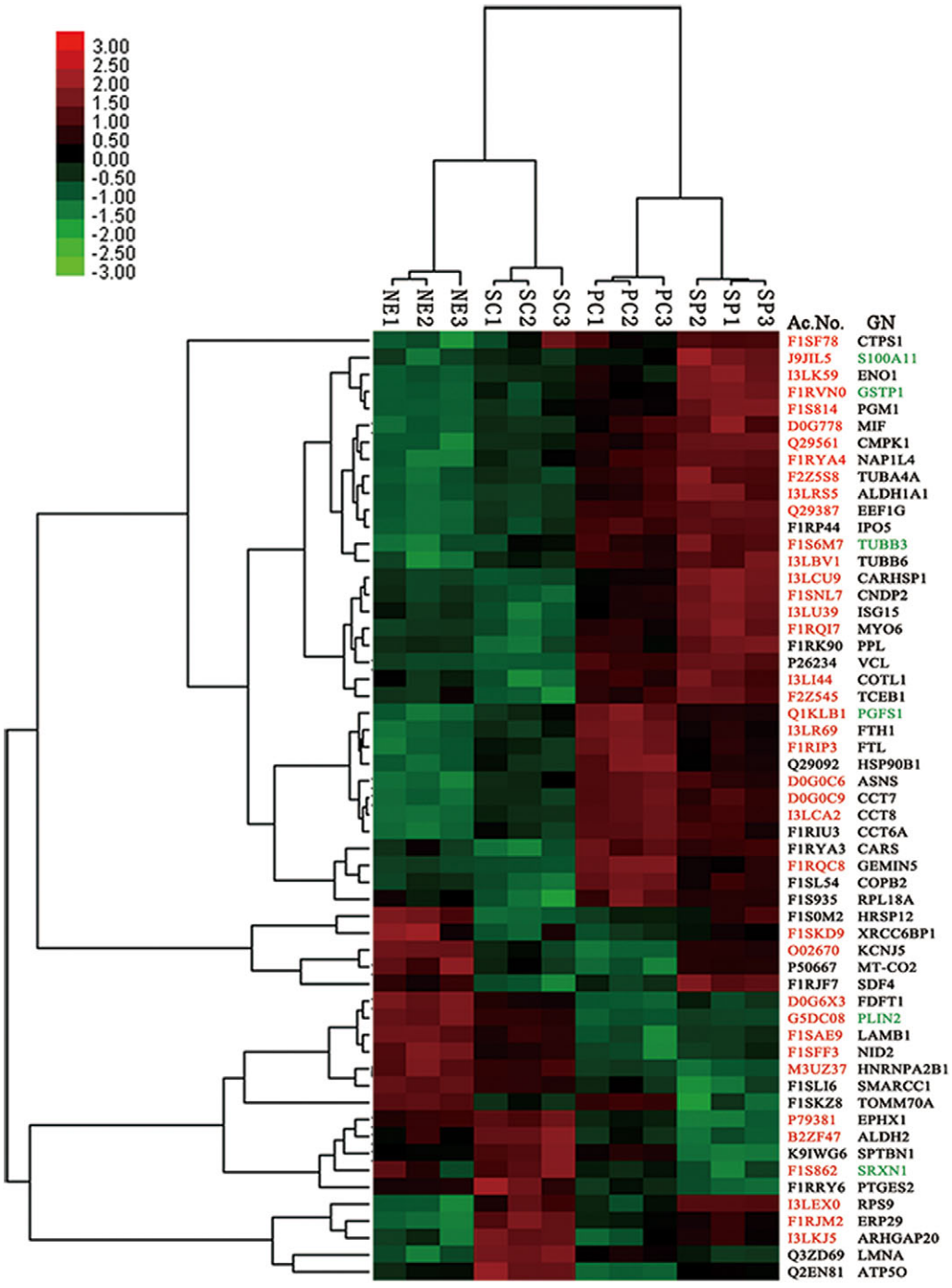

Figure 4. Heatmap of identified proteins based on hierarchical cluster analysis. Abundance profiles of proteins with selective features of NE, SP, SC, and PC groups were calculated in the context of all 3932 identified proteins after normalization using hierarchical cluster analysis. Ac. No. indicates the accession number of the respective protein in the UniProt database, and differentially abundant proteins are colored red. GN indicates the gene name for the corresponding protein, and proteins referenced in the GO database are colored green.

in the localization of central node proteins to mediate signal transduction in these biological pathways.

The above results suggest a number of functions, pathways and complicated molecular networks are affected when PCV2 was involved in the replication of CSFV in host cells, which further emphasizes the impact that PCV2 has on CSFV replication and the dominant role that PCV2 plays in PCV2-CSFV coinfection.

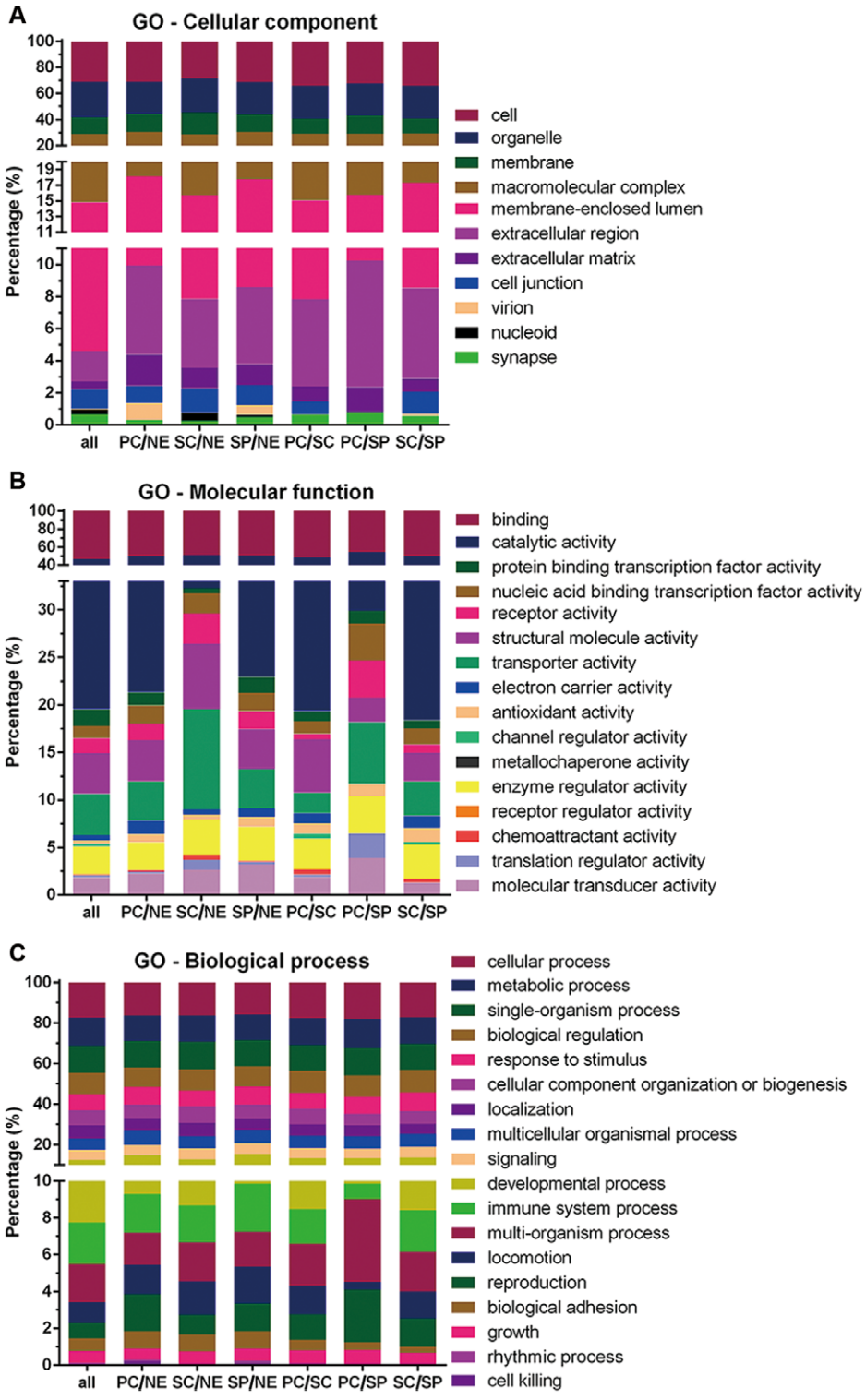

Figure 5. GO analysis of differentially abundant proteins. Annotations of cellular components, molecular functions and biological processes obtained from the GO database analyzed at level 2. All indicates all identified proteins, and others indicates proteins differentially abundant between groups.

3.8 Bioinformatic analysis of the differentially abundant proteins involved in PCV2-CSFV coinfection

To investigate the effect of PCV2-CSFV coinfection, a total of 184 proteins in clusters A7, B1, B2 and B3 (Fig. 2C) that were defined as differentially abundant during PCV2-CSFV coinfection were selected for further bioinformatic analysis. Of these, 94 were differentially abundant in PC/NE, 103 were differentially abundant in PC/SC, and 20 were differentially abundant in PC/SP, according to the Venn diagram (Fig. 8A). Notably, NADH-ubiquinone oxidoreductase chain 1 (ND1)

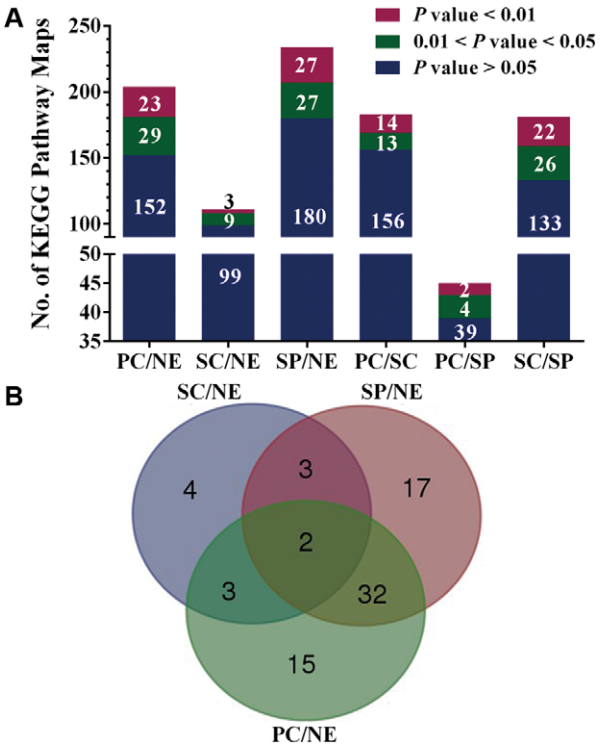

Figure 6. KEGG pathway analysis of differentially abundant proteins. Proteins differentially abundant between groups were blasted with KEGG GENES, retrieved their KEGG Orthology identifications (KOs) and subsequently mapped to pathways in KEGG. (A) Numbers of KEGG maps involved in proteins differentially abundant between groups. (B) Venn diagram analysis of KEGG pathway maps with statistical significance ($p < 0.05$) involved in SC/NE, SP/NE, and PC/NE.

was in all three groups. KEGG analysis revealed that the 94 differentially abundant proteins are involved in 145 KEGG pathways, 14 of which were statistically significant ($p < 0.05$; Table 1). These KEGG pathways (Table 1) overlapped with the 15 pathways identified in PC/NE alone (Supporting Information Table S7). Moreover, mitochondria were involved in many of the identified KEGG pathways, especially mitochondrial complexes of the electron transport chain, suggesting mitochondria might play an important role in PCV2-CSFV coinfection.

To investigate the molecular networks in which the differentially abundant proteins were involved, IPA was carried out as described above. In total, 177 differentially abundant proteins were matched in the IPA database, which covered 75 biological functions and 32 canonical pathways ($p > 0.05$; top 10 listed in Fig. 8B and 8C, respectively). The predominant biological functions identified as participating in PCV2-CSFV coinfection were developmental disorder, hereditary disorder and metabolic disease (Fig. 8B), and the major canonical pathways apparently influenced by PCV2-CSFV coinfection were oxidative phosphorylation, mitochondrial dysfunction and Nrf2-mediated oxidative stress response (Fig. 8C). Of note, the Z-score of Nrf2-mediated oxidative stress response category was 1, indicating that in particular, this pathway was activated during PCV2-CSFV coinfection (Fig. 8C).

Additionally, 11 molecular networks were constructed by IPA (Supporting Information Table S9). Figure 8D to 8G show the top four networks with the highest scores, and the categories were developmental disorder, hereditary disorder, metabolic disease, cellular assembly and organization, cell-to-cell signaling and interaction, reproductive system development and function, lipid metabolism, small molecule biochemistry, protein synthesis and hair and skin development and function. Additionally, as shown in Fig. 8D, complex I (Cx I), Cx IV and Cx V of the mitochondrial electron transport chain occupied centre nodes positions, and several subunits of these complexes were less abundant, such as MT-ND1, NDUFA12, NDUFA10, NDUFC2, NDUFS3 and NDUFB4, suggesting mitochondria may be the specifical target in PCV2-CSFV coinfection.

4 Discussion

Proteomic and bioinformatic analyses are powerful approaches for studying changes in global protein profiles during viral infection, and have been applied previously to investigate PCV2 [33–37] and CSFV [38,39] mono-infections in vivo and in vitro. Subsequent investigations on the less abundant tubulin proteins identified in proteomic analysis of PCV2 infection helped to establish a PCV2 transportation mechanism, and confirmed the important role of host cytoplasmic dynein systems for PCV2 infection [40]. Proteomic analysis can therefore help us to analyze and understand the mechanisms of viral infection, pathogenesis and host defense. In the present study, a coupled iTRAQ and LC-MS/MS approach was applied to explore the global proteome changes that occur during PCV2-CSFV coinfection, and the results were interpreted based on the existing in vitro PCV2-CSFV coinfection model [12]. Bioinformatic analysis revealed a dominant role for PCV2 in the major cellular processes specifically involved in PCV2-CSFV coinfection, and the results provide a basis for further investigation of the underlying molecular mechanisms.

4.1 Dominant role of PCV2 in PCV2-CSFV coinfection

The identification of proteins that were differentially abundant during viral infection illustrates the broad effects that PCV2 and CSFV have on host cellular protein abundance and cell physiology. Furthermore, hierarchical cluster, GO and KEGG analyses demonstrated the dominant role played by PCV2 in PCV2-CSFV-coinfected cells. Further investigation of 250 differentially abundant proteins in PC/SC using IPA showed that both PI3K/AKT signaling and Nrf2-mediated oxidative stress response were activated during PCV2-CSFV coinfection.

Conserved in all eukaryotic cells are 14-3-3 proteins that regulate a number of signaling-related ligand binding

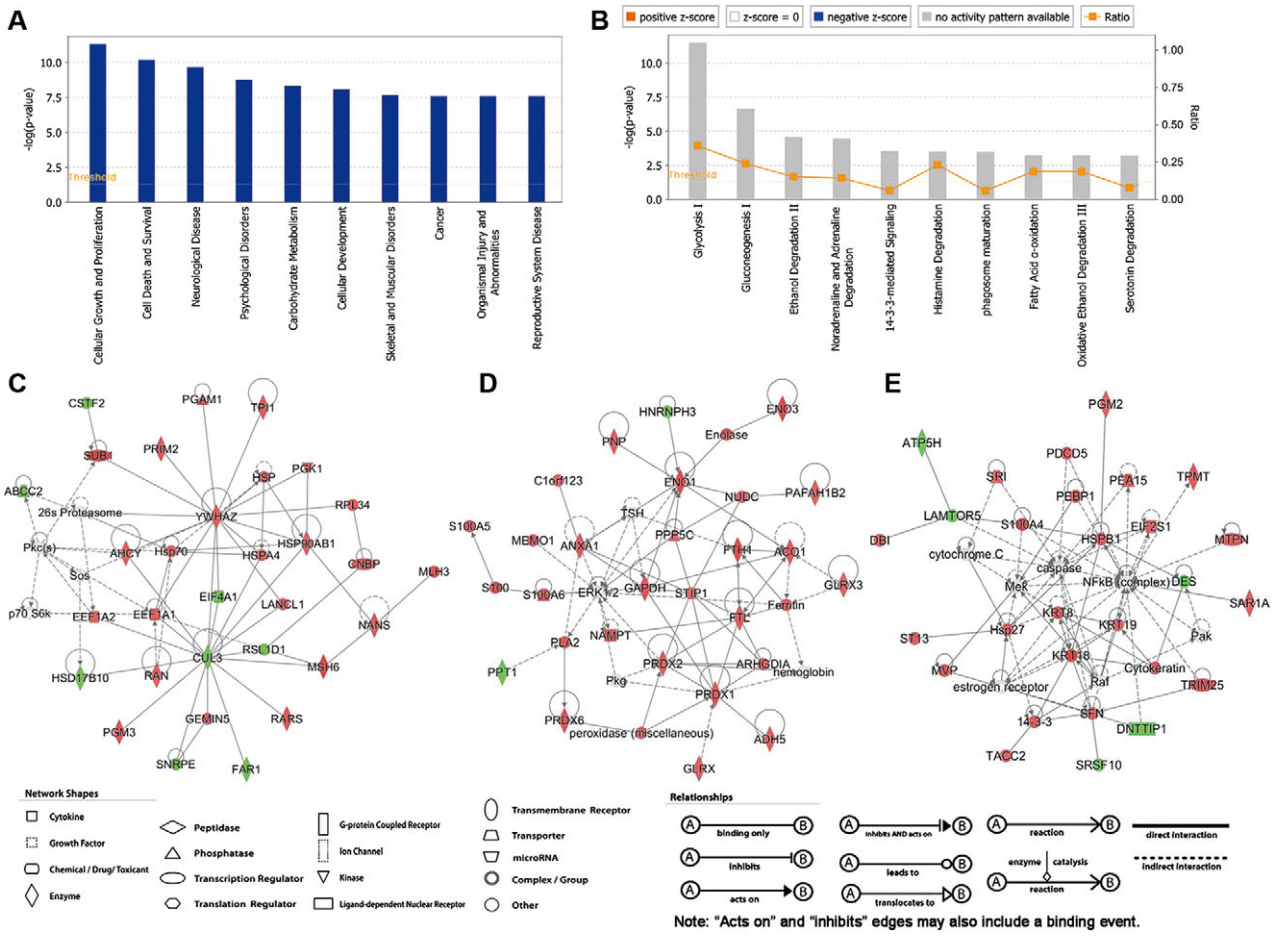

Figure 7. Dominant role of PCV2 in PCV2-CSFV coinfection confirmed by IPA. Analysis of differentially abundant proteins in PC/SC by IPA. Representative biological functions (A), canonical pathways (B) and molecular networks (C–E) are shown. The shapes of nodes represent different functional classes of genes and gene products. Proteins that increased and decreased their abundance in PC/SC are colored red and green, respectively. Lines between nodes represent interactions supported by at least one reference. These designations been used throughout.

proteins with diverse functions. Stimulation of the insulin-PI3K-AKT pathway in cells induces the interactome and results in dynamic changes of the 14-3-3 beta scaffold protein [41], indicating direct and indirect relationships between PI3K/AKT and 14-3-3 protein-induced signaling pathways. Activation of the PI3K/AKT signaling pathway during viral infection has been studied extensively [42–44]. Porcine aortic endothelial cells infected with CSFV displayed attenuated abundance of endothelial nitric oxide synthase and bioavailability of nitric oxide through activation of the ERK and PI3K/Akt pathways [45]. Meanwhile in PCV2-infected cells, the PI3K/AKT pathway plays an antiapoptotic role by preventing premature apoptosis that benefits PCV2 production [46] by limiting the extent of JNK1/2 and p38 activation and apoptosis signal-regulating kinase 1 [47]. However, in porcine alveolar macrophages, the PCV2 Cap protein interacts with gC1qR and activates the PI3K/Akt and p38 MAPK signaling pathways, and stimulates PCV2-induced IL-10 production [48]. In the present study, compared with CSFV mono-infection, the higher abundance of 14-3-3 σ encoded by SFN, 14-3-3 γ encoded by YWHAG, 14-3-3 ζ encoded by YWHAZ, and tubulin family members TUBB, TUBA4A, TUBB4B, and TUBB2B in PCV2-CSFV-coinfected cells is consistent with the involvement of PI3K/AKT and 14-3-3 signaling pathways. However, the abundance of kinases in the PI3K/AKT pathway did not noticeably alter. A reasonable explanation is that the regulatory function of these kinases may be dependent on post-translationally modified forms. Moreover, the differentially abundant proteins SFN, YWHAG and YWHAZ are also known to be involved in other signaling pathways, including Myc-mediated apoptosis signaling, ERK5 signaling, HIPPO signaling, p70S6K signaling and ERK/MAPK signaling pathways. However, the specific functions of these proteins in PCV2-CSFV coinfection or PCV2 mono-infection need further investigation.

Nrf2 binds to the small Maf protein and induces the transcription of phase II enzymes directly through antioxidant response elements (AREs) [49]. Normally, Nrf2 is located in the cytoplasm and degraded quickly. However, when cells are under oxidative stress, Nrf2 is phosphorylated by protein

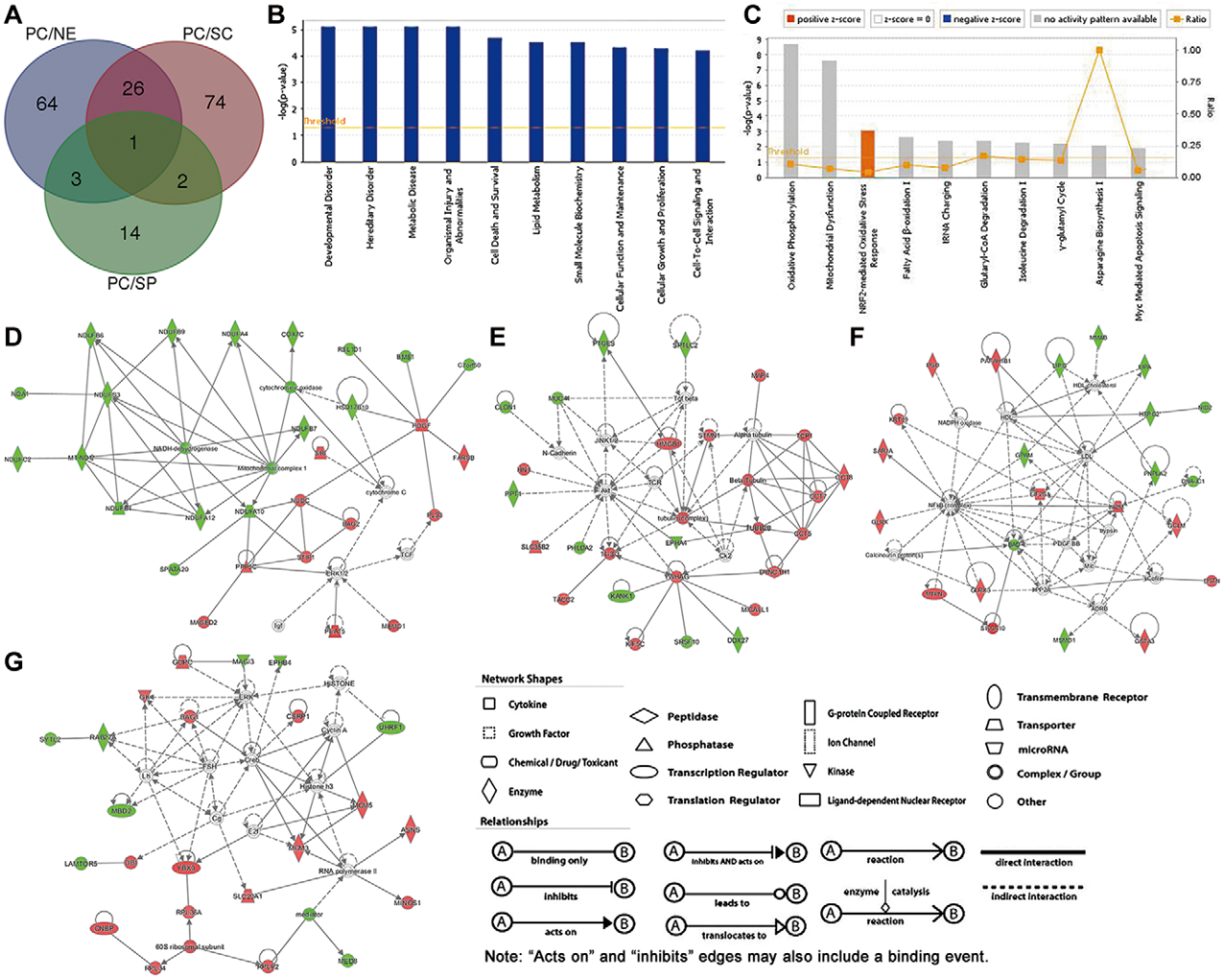

Figure 8. Bioinformatic analysis of the differentially abundant proteins during PCV2-CSFV coinfection. The differentially abundant proteins during PCV2-CSFV coinfectionwere defined and analyzed. (A) Venn diagram of differentially abundant proteins. (B-G) IPA of differentially abundant proteins. Representative biological functions (B), canonical pathways (C) and molecular networks (D–G) are shown.

kinase C and translocated into the nucleus where it regulates AREs [50]. Moreover, highly pathogenic influenza A viruses (IAV) induced a greater proportion of phosphorylated Nrf2 in the nucleus than did seasonal and pandemic strains [51], and Nrf2-deficent mice displayed increased abundance of oxidative and inflammatory genes when infected with IAV [52], indicating an important role for Nrf2 during IAV infection. A recent study showed that the porcine selenoprotein S protein blocked ochratoxin A-induced oxidative stress and impaired PCV2 replication by increasing mRNA levels of Nrf2 and other genes [53]. Notably, in the present study, compared with CSFV mono-infection, PCV2-CSFV coinfection resulted in a greater number of differentially abundant proteins associated with Nrf2-mediated oxidative stress response, including antioxidant proteins FTL, FTH1 and PRDX1, metabolizing enzymes GCLM and GSTA3, chaperone & stress response protein STIP1, detoxifying protein ABCC2, and ubiquitin ligase CUL3. Except for ABCC2 and CUL3, the others were more abundant, indicating activation of Nrf2-mediated oxidative stress response when PCV2 was involved in CSFV replication. The exact molecular mechanisms of Nrf2 and related proteins in PCV2 infection are certainly worth investigating in the future.

4.2 Physiological processes specifically involved in PCV2-CSFV coinfection

Mitochondria are important organelles that generate most cellular energy in the form of ATP via the electron transport chain (ETC) and its associated electrochemical proton gradient. The ETC, also known as the respiratory chain, comprises a series of protein complexes that transfer electrons from electron donors to electron acceptors, and this process links to several viral infections. For example, the core protein of HCV reduces the activity of electron transport protein Cx I and stimulates the production of ROS in liver mitochondria [54]. Similarly, patients coinfected with HIV and

Table 1. KEGG maps of the differentially abundant proteins in PCV2-CSFV coinfection

Map ID	Map name	%Test	%Ref	*p* value
ko05010	Alzheimer's disease	6.5217	2.1617	0.0004
ko04932	Non-alcoholic fatty liver disease (NAFLD)	5.4348	1.7294	0.0008
ko05012	Parkinson's disease	5.9783	2.1617	0.0013
ko00190	**Oxidative phosphorylation**	5.9783	2.1872	0.0014
ko00860	Porphyrin and chlorophyll metabolism	2.1739	0.3815	0.0038
ko03320	PPAR signaling pathway	2.7174	0.6612	0.0052
ko03030	**DNA replication**	2.1739	0.4832	0.0089
ko00561	**Glycerolipid metabolism**	2.1739	0.5341	0.0125
ko05016	Huntington's disease	5.4348	2.6704	0.0146
ko00830	**Retinol metabolism**	1.0870	0.1526	0.0270
ko05204	Chemical carcinogenesis	1.6304	0.4323	0.0354
ko04626	Plant–pathogen interaction	1.0870	0.1780	0.0361
ko00073	**Cutin, suberine, and wax biosynthesis**	0.5435	0.0254	0.0468
ko00626	**Naphthalene degradation**	0.5435	0.0254	0.0468

NOTE: "%Test" was the proportion of differentially abundant proteins of map in 184; "%Ref" was the proportion of proteins of map in all 3932 identified proteins. *P* value represented the statistical difference between differentially abundant proteins and maps. Bold represented KEGG maps newly identified here, and underline represented KEGG maps could be found in previously KEGG analysis.)

HCV display more serious metabolic aberrations in liver mitochondria due to compromised Cx IV activity than do patients infected with HCV alone [55]. Similarly, infection with rabies virus increases the activity of Cx I and Cx IV in neurons [56], and an increase in Cx I activity correlates with susceptibility to rabies virus infection and the presence of a rabies virus phosphoprotein, together with mitochondrial dysfunction and ROS generation [57]. However, regulation of the ETC during PCV2 or CSFV replication has not yet been reported. In this study, 13 proteins specifically involved in mitochondrial dysfunction by IPA were identified as differentially abundant in PCV2-CSFV-coinfected cells. Furthermore, ten subunits involved in this network that include Cx I, Cx II and Cx V, as well as ERK1/2 and cytochrome C, were less abundant during coinfection, but not to the extent that they could be considered as differentially abundant. These results indicated that mitochondria might be the main target for PCV2-CSFV coinfection, although the precise influence on mitochondria during viral infection needs further investigation.

Apoptosis induced by CSFV infection was found to be closely related to virulence. Attenuated CSFV strain vaccines induced apoptosis via 5' and 3' UTR features in the genome [58], while moderate and virulent forms of CSFV inhibited apoptosis through nonstructural proteins [59,60]. The protein encoded by ORF3 of PCV2 was reported to induce apoptosis by activating caspase-8 and caspase-3 pathways [61] and is believed to play an important role in PCV2-induced pathogenesis in vivo [62]. Recently, the PCV2 Cap protein was also reported to trigger cell death via various signaling pathways [63]. Our recent study revealed that the C strain of CSFV was unable to induce apoptosis in PK15 cells, whereas PCV2 replication could induce apoptosis and also impaired CSFV replication in PCV2-CSFV coinfection.

The Bcl-2-associated death promoter (BAD) is involved in apoptosis. Dephosphorylated BAD dissociates from 14-3-3 in the cytosol, translocates to mitochondria [64], dimerizes with the anti-apoptotic proteins Bcl-2 and Bcl-x(L) [65], and induces apoptosis. Influenza viruses subtly modulate activation of the apoptotic pathway by regulating BAD, and a failure to activate apoptosis results in nonproductive viral replication [66]. Moreover, BAD mRNA expression and protein abundance were found to be decreased by Epstein-Barr virus microRNA miR-BART20-5p, which contributes to tumorigenesis of Epstein-Barr virus-associated gastric carcinoma [67]. BAD was reported to be more abundant in apoptotic cells from the spleen tissue of PCV2-infected mice [68]. In the present study, BAD was found to be to be significantly less abundant during PCV2-CSFV coinfection. Thus, further investigation of the mechanism underlying lower abundance of BAD in PCV2-CSFV coinfectionis needed to better understand virus infection, host defences and viral interactions, which might help to prevent and control PCV2-CSFV coinfection in the field.

To our knowledge, the present study represents the first attempt to systematically analyze the protein abundance profiles of cells coinfected with PCV2 and CSFV using a coupled iTRAQ and LC-MS/MS approach and bioinformatic analysis. The results showed that PCV2 plays a dominant role in the differential abundance of host proteins during PCV2-CSFV coinfection. Moreover, analysis of the differentially abundant proteins during PCV2-CSFV coinfection suggested that mitochondrial dysfunction, Nrf2-mediated oxidative stress response, and apoptosis signaling pathways were involved in the coinfection of PCV2 and CSFV in host cells.

This work was supported by grants from the National Natural Science Foundation of China (Project No. 31230072, 31402198), the National Key Technology R & D Program of China (Grant No. 2015BAD12B01) and the Veterinary Etiological Biology State Key Laboratory (Grant No. 2015KFKT00812B01).

We thank Mrs. Yunqin Li in Institute of Agrobiology and Environmental Sciences of Zhejiang University for CLSM, Mr. Yang Zhang in Institutes of Biomedical Sciences of Fudan University and Shanghai Applied Protein Technology Co. Ltd for proteomic and bioinformatic analyses, and Mr. Gerhard Mayer and Mr. Andrew Jarnuczak in the PRIDE team for the submission of mass spectrometry proteomic data.

The authors have declared no conflict of interest.

5 References

[1] Birger, R. B., Kouyos, R. D., Cohen, T., Griffiths, E. C., Huijben, S., Mina, M., Volkova, V., Grenfell, B., Metcalf, C. J. E., *Trend. Microbiol.* 2015, *23*, 537–544.

[2] Liaw, Y. F., *Cancer J.* 1997, *10*, 189–192.

[3] Gao, R. B., Cao, B., Hu, Y. W., Feng, Z. J., Wang, D. Y., Hu, W. F., Chen, J., Jie, Z. J., Qiu, H. B., Xu, K., Xu, X. W., Lu, H. Z., Zhu, W. F., Gao, Z. C., Xiang, N. J., Shen, Y. Z., He, Z. B., Gu, Y., Zhang, Z. Y., Yang, Y., Zhao, X., Zhou, L., Li, X. D., Zou, S. M., Zhang, Y., Li, X. Y., Yang, L., Guo, J. F., Dong, J., Li, Q., Dong, L. B., Zhu, Y., Bai, T., Wang, S. W., Hao, P., Yang, W. Z., Zhang, Y. P., Han, J., Yu, H. J., Li, D. X., Gao, G. F., Wu, G. Z., Wang, Y., Yuan, Z. H., Shu, Y. L., *New Engl. J. Med.* 2013, *368*, 1888–1897.

[4] Chen, H. Y., Yuan, H., Gao, R. B., Zhang, J. X., Wang, D. Y., Xiong, Y., Fan, G. Y., Yang, F., Li, X. D., Zhou, J. F., Zou, S. M., Yang, L., Chen, T., Dong, L. B., Bo, H., Zhao, X., Zhang, Y., Lan, Y., Bai, T., Dong, J., Li, Q., Wang, S. W., Zhang, Y. P., Li, H., Gong, T., Shi, Y., Ni, X. S., Li, J. X., Zhou, J., Fan, J. Y., Wu, J. W., Zhou, X. F., Hu, M. H., Wan, J. G., Yang, W. Z., Li, D. X., Wu, G. Z., Feng, Z. J., Gao, G. F., Wang, Y., Jin, Q., Liu, M. B., Shu, Y. L., *Lancet* 2014, *383*, 714–721.

[5] Tong, S. X., Li, Y., Rivailler, P., Conrardy, C., Castillo, D. A. A., Chen, L. M., Recuenco, S., Ellison, J. A., Davis, C. T., York, I. A., Turmelle, A. S., Moran, D., Rogers, S., Shi, M., Tao, Y., Weil, M. R., Tang, K., Rowe, L. A., Sammons, S., Xu, X. Y., Frace, M., Lindblade, K. A., Cox, N. J., Anderson, L. J., Rupprecht, C. E., Donis, R. O., *Proc. Natl. Acad. Sci. USA* 2012, *109*, 4269–4274.

[6] Tong, S. X., Zhu, X. Y., Li, Y., Shi, M., Zhang, J., Bourgeois, M., Yang, H., Chen, X. F., Recuenco, S., Gomez, J., Chen, L. M., Johnson, A., Tao, Y., Dreyfus, C., Yu, W. L., McBride, R., Carney, P. J., Gilbert, A. T., Chang, J., Guo, Z., Davis, C. T., Paulson, J. C., Stevens, J., Rupprecht, C. E., Holmes, E. C., Wilson, I. A., Donis, R. O., *PLOS Pathogen.* 2013, *9*, 1078–1084.

[7] Hamel, A. L., Lin, L. L., Nayar, G. P. S., *J. Virol.* 1998, *72*, 5262–5267.

[8] Zhou, J. Y., Chen, Q. X., Ye, J. X., Shen, H. G., Chen, T. F., Shang, S. B., *Veterin. Res. Commun.* 2006, *30*, 205–220.

[9] Harding, J. C. S., Clark, E. G., *Swine Health Production* 1997, *5*, 201–203.

[10] Moennig, V., Plagemann, P. G. W., *Adv. Virus Res.* 1992, *41*, 53–98.

[11] Huang, Y.-L., Pang, V. F., Lin, C.-M., Tsai, Y.-C., Chia, M.-Y., Deng, M.-C., Chang, C.-Y., Jeng, C.-R., *Vet. Res.* 2011, *42*, 115.

[12] Zhou, N., Xing, G., Zhou, J. W., Jin, Y. L., Liang, C. Q., Gu, J. Y., Hu, B. L., Liao, M., Wang, Q., Zhou, J. Y., *Plos One* 2015, *10*, e0139457.

[13] Oxford, K. L., Wendler, J. P., McDermott, J. E., White, R. A., Powell, J. D., Jacobs, J. M., Adkins, J. N., Waters, K. M., *Expert Rev. Proteomics* 2016, *13*, 579–591.

[14] Zheng, X. J., Hong, L. L., Shi, L. X., Guo, J. Q., Sun, Z., Zhou, J. Y., *Mol. Cell. Proteomics* 2008, *7*, 612–625.

[15] Jiang, X. S., Tang, L. Y., Dai, J., Zhou, H., Li, S. J., Xia, Q. C., Wu, J. R., Zeng, R., *Mol. Cell. Proteomics* 2005, *4*, 902–913.

[16] Bartee, E., McCormack, A., Fruh, K., *PLOS Pathogen.* 2006, *2*, 975–988.

[17] Lietzen, N., Ohman, T., Rintahaka, J., Julkunen, I., Aittokallio, T., Matikainen, S., Nyman, T. A., *PLOS Pathogen.* 2011, *7*, 395–396.

[18] Luber, C. A., Cox, J., Lauterbach, H., Fancke, B., Selbach, M., Tschopp, J., Akira, S., Wiegand, M., Hochrein, H., O'Keeffe, M., Mann, M., *Immunity* 2010, *32*, 279–289.

[19] Wu, W. W., Wang, G. H., Baek, S. J., Shen, R. F., *J. Proteome Res.* 2006, *5*, 651–658.

[20] Mertins, P., Udeshi, N. D., Clauser, K. R., Mani, D., Patel, J., Ong, S.-E., Jaffe, J. D., Carr, S. A., *Mol. Cell. Proteomics* 2012, *11*, 1377–1391.

[21] Gan, C. S., Chong, P. K., Pham, T. K., Wright, P. C., *J. Proteome Res.* 2007, *6*, 821–827.

[22] Zhou, J. Y., Shang, S. B., Gong, H., Chen, Q. X., Wu, J. X., Shen, H. G., Chen, T. F., Guo, J. Q., *J. Biotechnol.* 2005, *118*, 201–211.

[23] Shang, S. B., Jin, Y. L., Jiang, X. T., Zhou, J. Y., Zhang, X., Xing, G., He, J. L., Yan, Y., *Mol. Immunol.* 2009, *46*, 327–334.

[24] Lin, M., Lin, F., Mallory, M., Clavijo, A., *J. Virol.* 2000, *74*, 11619–11625.

[25] Wisniewski, J. R., Zougman, A., Nagaraj, N., Mann, M., *Nat. Methods* 2009, *6*, 359–362.

[26] Sun, Y. T., Hu, B. L., Fan, C. F., Jia, L., Zhang, Y. N., Du, A. F., Zheng, X. J., Zhou, J. Y., *Electrophoresis* 2015, *36*, 1596–1611.

[27] Vizcaino, J. A., Deutsch, E. W., Wang, R., Csordas, A., Reisinger, F., Rios, D., Dianes, J. A., Sun, Z., Farrah, T., Bandeira, N., Binz, P. A., Xenarios, I., Eisenacher, M., Mayer, G., Gatto, L., Campos, A., Chalkley, R. J., Kraus, H. J., Albar, J. P., Martinez-Bartolome, S., Apweiler, R., Omenn, G. S., Martens, L., Jones, A. R., Hermjakob, H., *Nat. Biotechnol.* 2014, *32*, 223–226.

[28] Vizcaino, J. A., Csordas, A., del-Toro, N., Dianes, J. A., Griss, J., Lavidas, I., Mayer, G., Perez-Riverol, Y., Reisinger, F., Ternent, T., Xu, Q. W., Wang, R., Hermjakob, H., *Nucleic Acids Res.* 2016, *44*, D447–D456.

[29] Hall, Mark, Frank, Eibe, Holmes, Geoffrey, Pfahringer, Bernhard, Reutemann, Peter, *AcmSigkdd Explorations Newsletter* 2010, *11*, 10–18.

[30] Eisen, M. B., Spellman, P. T., Brown, P. O., Botstein, D., *Proc. Natl. Acad. Sci. USA* 1998, *95*, 14863–14868.

[31] Ye, C. J., Jia, L., Sun, Y. T., Hu, B. L., Wang, L., Lu, X. M., Zhou, J. Y., *J. Virol.* 2014, *88*, 11154–11165.

[32] Chae, C., *Vet. J.* 2005, *169*, 326–362.

[33] Zhang, X., Zhou, J. Y., Wu, Y. P., Zheng, X. J., Ma, G. P., Wang, Z. T., Jin, Y. L., He, J. L., Yan, Y., *J. Proteome Res.* 2009, *8*, 5111–5119.

[34] Ramirez-Boo, M., Nunez, E., Jorge, I., Navarro, P., Fernandes, L. T., Segales, J., Garrido, J. J., Vazquez, J., Moreno, A., *Proteomics* 2011, *11*, 3452–3469.

[35] Cheng, S., Zhang, M., Li, W., Wang, Y., Liu, Y., He, Q., *J. Proteomics* 2012, *75*, 3258–3269.

[36] Liu, J., Bai, J., Lu, Q., Zhang, L., Jiang, Z., Michal, J. J., He, Q., Jiang, P., *J. Proteomics* 2013, *79*, 72–86.

[37] Marco-Ramell, A., Miller, I., Noebauer, K., Moeginger, U., Segales, J., Razzazi-Fazeli, E., Kolarich, D., Bassols, A., *J. Proteomics* 2014, *101*, 205–216.

[38] Sun, J., Jiang, Y., Shi, Z., Yan, Y., Guo, H., He, F., Tu, C., *J. Proteome Res.* 2008, *7*, 5263–5269.

[39] Sun, J., Shi, Z., Guo, H., Tu, C., *J. Gen. Virol.* 2010, *91*, 2254–2262.

[40] Cao, J., Lin, C., Wang, H., Wang, L., Zhou, N., Jin, Y., Liao, M., Zhou, J., *J. Virol.* 2015, *89*, 2777–2791.

[41] Collins, B. C., Gillet, L. C., Rosenberger, G., Roest, H. L., Vichalkovski, A., Gstaiger, M., Aebersold, R., *Nat. Methods* 2013, *10*, 1246–1253.

[42] Ehrhardt, C., Wolff, T., Pleschka, S., Planz, O., Beermann, W., Bode, J. G., Schmolke, M., Ludwig, S., *J. Virol.* 2007, *81*, 3058–3067.

[43] Portis, T., Longnecker, R., *Oncogene* 2004, *23*, 8619–8628.

[44] Mannova, P., Beretta, L., *J. Virol.* 2005, *79*, 8742–8749.

[45] Wang, C. Y., Yeh, H. I., Chang, T. J., Hsiao, H. J., Tsai, M. S., Tsai, S. M., Liu, P. A., *Arch. Virol.* 2011, *156*, 1151–1160.

[46] Wei, L., Zhu, S., Wang, J., Liu, J., *J. Virol.* 2012, *86*, 13589–13597.

[47] Wei, L., Zhu, S., Wang, J., Zhang, C., Quan, R., Yan, X., Liu, J., *Virology* 2013, *447*, 285–291.

[48] Du, Q., Huang, Y., Wang, T., Zhang, X., Chen, Y., Cui, B., Li, D., Zhao, X., Zhang, W., Chang, L., Tong, D., *Oncotarget* 2016, *7*, 17492–17507.

[49] Itoh, K., Chiba, T., Takahashi, S., Ishii, T., Igarashi, K., Katoh, Y., Oyake, T., Hayashi, N., Satoh, K., Hatayama, I., Yamamoto, M., Nabeshima, Y., *Biochem. Biophys. Res. Commun.* 1997, *236*, 313–322.

[50] Huang, H. C., Nguyen, T., Pickett, C. B., *J. Biol. Chem.* 2002, *277*, 42769–42774.

[51] Simon, P. F., McCorrister, S., Hu, P., Chong, P., Silaghi, A., Westmacott, G., Coombs, K. M., Kobasa, D., *J. Proteome Res.* 2015, *14*, 4511–4523.

[52] Yageta, Y., Ishii, Y., Morishima, Y., Masuko, H., Ano, S., Yamadori, T., Itoh, K., Takeuchi, K., Yamamoto, M., Hizawa, N., *J. Virol.* 2011, *85*, 4679–4690.

[53] Gan, F., Hu, Z., Huang, Y., Xue, H., Huang, D., Qian, G., Hu, J., Chen, X., Wang, T., Huang, K., *Oncotarget* 2016, *7*, 20469–20485.

[54] Korenaga, M., Wang, T., Li, Y. C., Showalter, L. A., Chan, T. S., Sun, J. R., Weinman, S. A., *J. Biol. Chem.* 2005, *280*, 37481–37488.

[55] Chapplain, J. M., Tattevin, P., Guyader, D., Begue, J. M., Beillot, J., Turlin, B., Souala, F., Arvieux, C., Rochcongar, P., Michelet, C., *HivClin. Trials* 2011, *12*, 54–60.

[56] Alandijany, T., Kammouni, W., Chowdhury, S. K. R., Fernyhough, P., Jackson, A. C., *J. Neurovirol.* 2013, *19*, 537–549.

[57] Kammouni, W., Wood, H., Saleh, A., Appolinario, C. M., Fernyhough, P., Jackson, A. C., *J. Neurovirol.* 2015, *21*, 370–382.

[58] Hsu, W. L., Chen, C. L., Huang, S. W., Wu, C. C., Chen, I. H., Nadar, M., Su, Y. P., Tsai, C. H., *PLoS One* 2014, *9*, e88863.

[59] Ruggli, N., Bird, B. H., Liu, L., Bauhofer, O., Tratschin, J. D., Hofmann, M. A., *Virology* 2005, *340*, 265–276.

[60] Tang, Q., Guo, K., Kang, K., Zhang, Y., He, L., Wang, J., *Virus Genes* 2011, *42*, 355–362.

[61] Liu, J., Chen, I., Kwang, J., *J. Virol.* 2005, *79*, 8262–8274.

[62] Liu, J., Chen, I., Du, Q. Y., Chua, H. K., Kwang, J., *J. Virol.* 2006, *80*, 5065–5073.

[63] Walia, R., Dardari, R., Chaiyakul, M., Czub, M., *Virology* 2014, *468*, 126–132.

[64] Wang, H. G., Pathan, N., Ethell, I. M., Krajewski, S., Yamaguchi, Y., Shibasaki, F., McKeon, F., Bobo, T., Franke, T. F., Reed, J. C., *Science* 1999, *284*, 339–343.

[65] Kelekar, A., Chang, B. S., Harlan, J. E., Fesik, S. W., Thompson, C. B., *Mol. Cell. Biol.* 1997, *17*, 7040–7046.

[66] Tran, A. T., Cortens, J. P., Du, Q., Wilkins, J. A., Coombs, K. M., *J. Virol.* 2013, *87*, 1049–1060.

[67] Kim, H., Choi, H., Lee, S. K., *Cancer Lett.* 2015, *356*, 733–742.

[68] Kiupel, M., Stevenson, G. W., Galbreath, E. J., North, A., HogenEsch, H., Mittal, S. K., *BMC Vet. Res.* 2005, *1*, 1–8.

